Enhanced Slow Inactivation by V445M: A Sodium Channel Mutation Associated with Myotonia

Masanori P. Takahashi* and Stephen C. Cannon*#
*Department of Neurology, Massachusetts General Hospital, and #Department of Neurobiology, Harvard Medical School, Boston, MA 02114 USA

ABSTRACT Over 20 different missense mutations in the α subunit of the adult skeletal muscle Na channel have been identified in families with either myotonia (muscle stiffness) or periodic paralysis, or both. The V445M mutation was recently found in a family with myotonia but no weakness. This mutation in transmembrane segment IS6 is novel because no other disease-associated mutations are in domain I. Na currents were recorded from V445M and wild-type channels transiently expressed in human embryonic kidney cells. In common with other myotonic mutants studied to date, fast gating behavior was altered by V445M in a manner predicted to increase excitability: an impairment of fast inactivation increased the persistent Na current at 10 ms and activation had a hyperpolarized shift (4 mV). In contrast, slow inactivation was enhanced by V445M due to both a slower recovery (10 mV left shift in β(V)) and an accelerated entry rate (1.6-fold). Our results provide additional evidence that IS6 is crucial for slow inactivation and show that enhanced slow inactivation cannot prevent myotonia, whereas previous studies have shown that disrupted slow inactivation predisposes to episodic paralysis.

INTRODUCTION

Voltage-gated Na channels are the primary determinant of excitability in skeletal and heart muscle and in neurons. Excitability is strongly dependent on intrinsic gating properties of Na channels, and inactivation—a decline in Na current despite a maintained membrane depolarization—is a universal feature of all voltage-gated Na channels. Fast inactivation operates on a time scale of milliseconds and alters the availability of Na channels over the time course of a single action potential. Slow inactivation occurs on a time scale of seconds to minutes and may modulate excitability in response to slow shifts in the resting potential (Chandler and Meves, 1970; Almers et al., 1983; Ruff et al., 1988). Defects of inactivation have recently been identified in mutant human Na channels that cause disorders of skeletal muscle (Cannon, 1998) or heart (Ackerman, 1998). In this study we have identified a novel enhancement of slow inactivation by V445M, a missense mutation associated with myotonia that is predicted to lie in the S6 segment of domain I (Rosenfeld et al., 1997).

More than 20 missense mutations in the α subunit of the adult human skeletal muscle Na channel (hSkM1) are known to cause several heritable muscle diseases including hyperkalemic periodic paralysis (HyperPP), paramyotonia congenita (PMC), and potassium-aggravated myotonia (PAM). The functional consequences of these mutations have been investigated in order to understand the pathophysiological basis for the enhanced excitability in myotonia and the inexcitability during attacks of periodic paralysis. Fast inactivation is partially disrupted by every mutation tested to date (Cannon, 1997) and a subset of mutations also cause a hyperpolarized shift in activation (Cummins et al., 1993; Mitrovic et al., 1995; Green et al., 1998; Plassart-Schiess et al., 1998). In model simulations these functional defects are sufficient to cause the repetitive discharges that give rise to myotonia and may cause paralysis in the more severely disrupted mutants by a depolarization-induced loss of excitability (Cannon et al., 1993; Hayward et al., 1996). Slow inactivation has recently been recognized as an additional determinant of the pathophysiology of these disorders (Ruff, 1994; Cannon, 1996; Cummins and Sigworth, 1996). Mutations that impair slow inactivation and alter fast-gating transitions occur in families in which weakness is a prominent feature (HyperPP). This association and model simulations both suggest that slow inactivation may normally protect muscle from prolonged depolarized shifts in the resting potential caused by a persistent Na current conducted by Na channels with altered fast-gating (Cummins and Sigworth, 1996; Hayward et al., 1997).

A novel missense mutation was recently identified in a family with recurrent attacks of painful myotonic stiffness but no episodic weakness (Rosenfeld et al., 1997). Valine 445, which lies in S6 of domain I and is conserved in the Na channels of most species from jellyfish to humans, was mutated to methionine. None of the other 20 missense mutations in hSkM1 associated with diseases of skeletal muscle occurs in domain I. We have transiently expressed V445M in mammalian cells and have detected changes in gating behavior. In agreement with a preliminary study by Bennett et al. (1998), we observed a mild disruption of fast inactivation and a small hyperpolarized shift of activation. More importantly, we also identified a pronounced enhancement of slow inactivation produced by an impediment to recovery (hyperpolarized shift in the voltage dependence of recovery) and a faster entry rate (~1.6-fold). This is the

Received for publication 6 August 1998 and in final form 3 November 1998.

Address reprint requests to Dr. Stephen C. Cannon, EDR 413, Massachusetts General Hospital, Boston, MA 02114. Tel.: 617-724-3531; Fax: 617-726-3926; E-mail: cannon@helix.mgh.harvard.edu.

0006-3495/99/02/861/08 $2.00

first example of a disease-related mutation that enhances slow inactivation and has implications for the pathogenesis of myotonia and weakness. Moreover, V445 is the second site in IS6 that augments slow inactivation when mutated. Wang and Wang (1997) showed that N434A in rat SkM1 (equivalent to N440A in hSkM1) speeds entry and slows recovery from slow inactivation. Although the molecular mechanism of slow inactivation remains unknown, these studies provide new evidence that IS6 has an important role in slow inactivation.

MATERIALS AND METHODS

Expression of sodium channels

The adult isoform of the human skeletal muscle sodium channel α-subunit, hSkM1 (George et al., 1992), and the mutant V445M were provided by Al George, Jr. These cDNAs were subcloned between the *Not*I and *Xba*I sites of the mammalian expression vector pRc/CMV. The human β subunit cDNA (McClatchey et al., 1993) was subcloned into the *Eco*RI site of the mammalian expression vector pcDNAI (Invitrogen, San Diego, CA).

Culture of human embryonic kidney (HEK) cells and their transient transfection were performed as described previously (Hayward et al., 1996). In brief, plasmid DNAs encoding wild-type (WT) or mutant human Na channel α subunits (0.9 μg/35-mm dish), the human Na channel β subunit (fourfold molar excess over α subunit DNA), and a CD8 marker (0.175 μg) were cotransfected by the calcium phosphate method. At 1–3 days after transfection, the HEK cells were trypsinized briefly and passaged to 22-mm round glass coverslips for electrophysiological recording. Individual transfection-positive cells were identified by labeling with anti-CD8 antibody cross-linked to microbeads (Dynal, Great Neck, NY) (Jurman et al., 1994).

Whole-cell recording

Na currents were measured using conventional whole-cell recording techniques as described previously (Hayward et al., 1996). Recordings were made with an Axopatch 200A amplifier (Axon Instruments, Foster City, CA). The output was filtered at 5 kHz and digitally sampled at 40 kHz using an LM900 interface (Dagan, Minneapolis, MN). Data were stored to a 486-based computer using a custom AxoBasic (Axon Instruments, Foster City, CA) data acquisition program. More than 80% of the series resistance was compensated by the analog circuitry of the amplifier and the leakage conductance was corrected by digital scaling and subtraction of the passive current elicited by a 20-mV depolarization from the holding potential. Cells with peak currents of < 1 nA or > 20 nA upon step depolarization from -120 mV to -10 mV were excluded. After initially establishing whole-cell access, we often observed leftward shifts in the voltage dependence of gating, an increase in the size of the peak current, and a decrease in the amplitude of persistent Na current. To minimize these effects, we waited at least 10 min for equilibration after gaining access to the cells.

Patch electrodes were fabricated from borosilicate capillary tubes with a multistage puller (Sutter, Novato, CA). The shank of the pipette was coated with Sylgard and the tip was heat-polished to a final tip resistance (in bath solution) of 0.5–2.0 MΩ. The pipette (internal) solution contained 105 mM CsF, 35 mM NaCl, 10 mM EGTA, and 10 mM Cs-HEPES (pH 7.4). Fluoride was used in the pipette to prolong seal stability. The bath contained 140 mM NaCl, 4 mM KCl, 2 mM $CaCl_2$, 1 mM $MgCl_2$, 5 mM glucose, and 10 mM Na-HEPES (pH 7.4). Recordings were made at room temperature (21–23 C°). Tetrodotoxin (TTX) was purchased from Sigma (St. Louis, MO).

Data analysis

Curve fitting was performed manually off-line using AxoBasic, SigmaPlot (Jandel Scientific, San Rafael, CA), or Origin (Microcal, Northhampton, MA). Conductance was calculated as $G(V) = I_{peak}(V)/(V - E_{rev})$, where the reversal potential, E_{rev}, was measured experimentally for each cell. Steady-state fast and slow inactivation were fitted to a Boltzmann function with a nonzero pedestal, I_o, calculated as $I/I_{peak} = (1 - I_o)/[1 + \exp((V - V_{1/2})/k)] + I_o$, where $V_{1/2}$ is the half-maximum voltage and k is the slope factor (Table 1). Symbols with error bars indicate means $\pm$ SEM. Statistical significance was determined by the unpaired t-test with p values noted in text.

RESULTS

Fast-gating transitions were altered by V445M

The kinetics of Na channel gating were characterized by recording whole-cell currents from HEK cells transiently transfected with cDNAs encoding WT or mutant (V445M) hSkM1, and the human isoform of the β subunit. Bennett et al. (1998) have reported, in abstract form, that fast inactivation is altered by V445M. We confirmed many of their observations, as briefly described below.

The voltage dependence of steady-state fast inactivation, $h_\infty(v)$, was measured with a 100-ms conditioning pulse, in order to minimize the effect of entry to the slow inactivated state (see below). The relative peak currents elicited at -10 mV were fit with a Boltzmann function, and the estimated parameter values are listed in Table 1. Mutant V445M had a -5 mV leftward (hyperpolarized) shift in the midpoint ($p < 0.0001$), whereas there was no difference in the steepness.

The amplitude of the persistent Na current, I_{ss} was evaluated by measuring the TTX-sensitive component with a subtraction protocol. The current elicited by a 10-ms step depolarization from -120 mV to -10 mV in the presence of 5 μM TTX was subtracted from that in normal external solution. The amplitude of steady-state current during the last 0.2 ms of the pulse was averaged and normalized to the peak value. I_{peak} V445M channels had an increased persistent current at 10 ms (0.70%) compared to WT (0.05%).

The voltage dependence of activation was measured by applying step depolarizations from -120 mV. The Na con-

TABLE 1 Parameter estimates for WT and V445M

	Activation, ($G(v)$)			Fast inactivation, $h_\infty(v)$		Slow inactivation, $S_\infty(v)$		
Mutation	$V_{1/2}$	k	I_{ss}/I_{peak}	$V_{1/2}$	k	$V_{1/2}$	k	S_0
	mV	mV/*e*-fold	%	mV	mV/*e*-fold	mV	mV/*e*-fold	
WT	-26.8 ± 1.1 (25)	5.3 ± 0.2	0.05 ± 0.02 (4)	-69.1 ± 1.0 (21)	5.2 ± 0.2	-64.2 ± 1.0 (6)	7.9 ± 0.5	0.16 ± 0.04
V445M	-30.9 ± 0.9 (26)	6.4 ± 0.3	0.70 ± 0.36 (4)	-74.0 ± 0.6 (25)	5.0 ± 0.1	-73.6 ± 1.4 (6)	6.6 ± 0.5	0.08 ± 0.01

ductance was estimated from the peak current and the measured reversal potential, E_{rev}, as $G(V) = I_{peak}(V)/(V - E_{rev})$. The conductance data were fit with a Boltzmann function and the estimated parameters are listed in Table 1. The V445M mutant had a −4 mV leftward (hyperpolarized) shift in the midpoint ($p < 0.002$).

Thus far, our observations on the effects of V445M on fast-gating are in agreement with those reported by Bennett et al. (1998). In addition, Bennett et al. (1998) found that recovery from inactivation was profoundly slowed for V445M. This was unexpected because other myotonia-associated mutations in hSkM1 accelerated the recovery from fast inactivation, whereas a sluggish recovery rate reduces the excitability of the cell. In their recovery protocol, Bennett et al. (1998) used a 500-ms conditioning pulse, which would cause a significant degree of slow, as well as fast, inactivation. We used a series of conditioning pulse durations to separate the effects of V445M on fast and slow inactivation.

Recovery from inactivation was tested using the three-pulse protocol shown in the inset of Fig. 1 *A*. Cells were held at −120 mV, and a conditioning pulse to −10 mV was applied for a preset duration. The conditioning pulse was followed by recovery at −120 mV for 0.05 to 10,000 ms. Peak Na current was measured in response to a subsequent test depolarization to −10 mV. Channel availability was measured as the ratio of the peak current during the test depolarization to that during the reference pulse. Traces in Fig. 1 *A* show example data for WT and V445M channels obtained with 300 ms conditioning pulses. The I_{Na} elicited at −10 mV after recovery times of 0.1, 3, 15, 70, and 10,000 ms were normalized to the peak of reference current and superimposed. Within 15 ms, 65% of the current recovered in WT channels but only 50% was available for V445M channels. The time course of recovery at −120 mV, after a series of conditioning pulses to −10 mV, is shown for WT and V445M in Fig. 1 *B*. Solid lines show fits to a two-exponential relaxation for visual guidance. For brief (30-ms) conditioning pulse intervals, more than 90% of the current for both WT and V445M channels recovered within 15 ms (inset, Fig. 1 *B*), indicating that the rapid monoexponential recovery from fast inactivation was indistinguishable for the two channel types. With longer conditioning pulse intervals (300 and 3000 ms), however, the time course of recovery of V445M channels was slower than that of WT. Recovery followed a multi-exponential time course after these prolonged conditioning pulses due to slow inactivation of channels. The sluggishness of the V445M channels was caused by a higher proportion of channels being slow-inactivated (lower amplitude of the fast component of

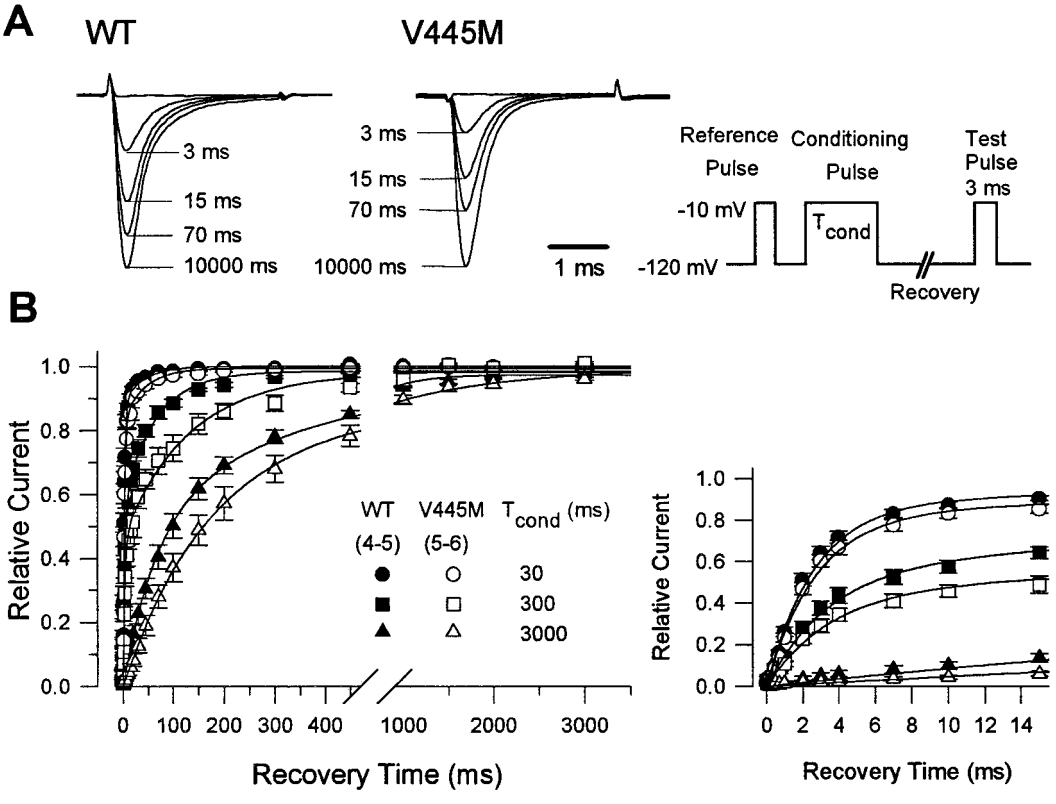

FIGURE 1 Recovery from inactivation was slowed for V445M channels. (*A*) A three-pulse protocol (*inset*) was used to measure recovery from inactivation as the fraction of available I_{Na}. Traces show currents for wild-type and V445M channels after a 300-ms conditioning pulse at −10 mV. I_{Na} elicited at −10 mV, after recovery times of 0.1, 3, 15, 70, and 10,000 ms, was normalized to the peak of reference current (12.4 nA for WT and 16.9 nA for V445M). (*B*) Relative current from WT and V445M channels is plotted as a function of the duration of recovery at −120 mV. Smooth curves are χ^2 minimized fits with double-exponential relaxation to averaged data and are shown for visual guidance.

recovery, Fig. 1 *B* inset) and by a slower recovery rate from the slow-inactivated state (Fig. 1 B). These data suggest that V445M alters slow inactivation, rather than a slowing of the recovery from fast inactivation suggested by Bennett et al. (1998).

Slow inactivation was enhanced by V445M

The voltage dependence of entry to slow inactivation was tested using the three pulse protocol shown in the inset of Fig. 2. Cells were held at −120 mV, and a conditioning pulse with varying duration was applied. Channel availability was measured as the ratio of the peak current during the test depolarization to that during the reference pulse. Between the reference and conditioning pulse the cell was held at −120 mV for 500 ms. Three different conditioning potentials (−90, −70, and −40 mV) were tested. The conditioning and test pulses were separated by a 20-ms hyperpolarization to −120 mV to allow recovery from fast inactivation. The kinetics of entry to slow inactivation at different membrane potentials are shown in Fig. 2. The entry to slow inactivation for both the WT and V445M channels was quicker and more complete at more depolarized potentials. For the V445M channels, however, slow inactivation developed more quickly than for WT channels. The time course of entry was fit to a single-exponential for each cell. The means of the estimated parameter values were used to generate curves in Fig. 2 and are plotted in Fig. 5 *C*. The time constant of WT channels at −90 mV is not shown in Fig. 5 *C*, because a reliable fit was difficult due to the small amplitude of the decay (see Fig. 2).

Data from the entry to slow inactivation protocol also enabled us to define the voltage dependence of steady-state slow inactivation, S_∞. As shown in Fig. 2, the extent of entry to slow inactivation approached a constant value within 60 s. The voltage dependence of S_∞ is shown for WT and V445M mutant channels in Fig. 3. Steady-state slow inactivation was measured using a 60-s prepulse, followed by a 20-ms gap at −120 mV to allow recovery from fast inactivation, before the −10 mV test pulse (inset). The voltage dependence of slow inactivation in V445M channels was steeper, shifted to the left (hyperpolarized) and more complete than WT. The data in Fig. 3 were fitted by a single Boltzmann plus a constant term, and estimated parameter values were listed in Table 1.

The voltage dependence of recovery from slow inactivation was measured for WT and V445M channels at −80, −100, and −120 mV. The voltage protocol is shown in the inset of Fig. 4. In this protocol, the holding and recovery potentials were identical so that the reference I_{Na} and test I_{Na} were elicited from the same starting potential. The recovery from slow inactivation in both the WT and V445M channels was quicker and more complete at more hyperpolarized potentials. For the WT channels, however, recovery from slow inactivation was faster than for V445M channels. A quantitative comparison was made by fitting the time course of the recovery data to a single exponential. Because this protocol measures the total recovery (both nonslow and slow inactivated channels), a fractional offset was used in the exponential fit. The fraction of channels not slow inactivated was set equal to the mean of the S_∞ data at −10mV (0.15 for WT and 0.07 for V445M). The smooth curves were generated with mean parameter values from fitting the data of each cell to a single-exponential relaxation. This single-exponential approximation for recovery was suboptimal, as discussed previously (Hayward et al., 1997), and a two- or three-exponential approximation was more accurate. We employed a single-exponential approximation, however, because it is representative of the majority of the current recovery and allows a single parameter comparison.

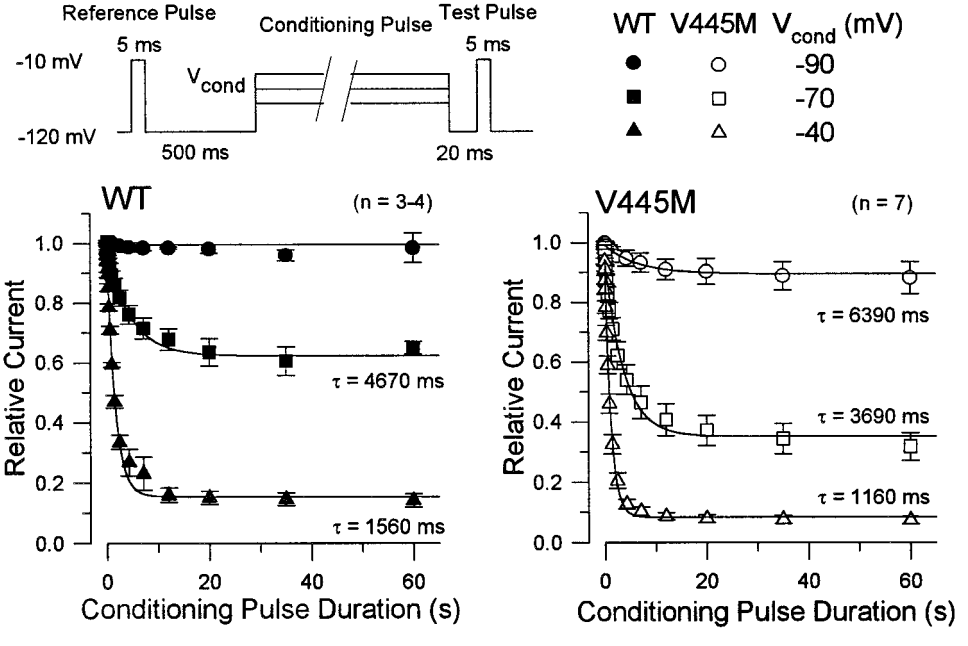

FIGURE 2 Entry to slow inactivation was enhanced for V445M channels. Entry to slow inactivation was measured as the peak I_{Na} elicited at −10 mV, after a conditioning pulse of variable duration (*inset*). Current amplitudes were normalized to the reference peak current elicited from a holding potential of −120 mV. The conditioning and test pulses were separated by a 20-ms hyperpolarization to −120 mV to allow channels to recover from fast inactivation. Symbols denote different conditioning voltages, and the smooth curves are generated with mean parameter values from χ^2 minimized fits of a single-exponential relaxation plus a constant to the data of each cell.

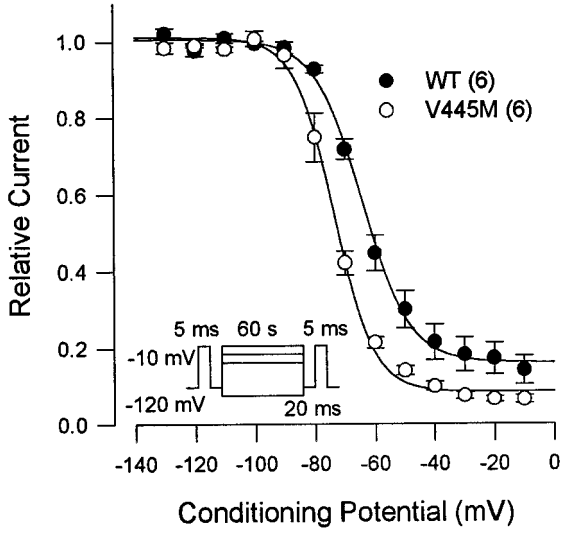

FIGURE 3 Steady-state slow inactivation was augmented for V445M channels. Steady-state slow inactivation was measured as the peak I_{Na} elicited at −10 mV after a 60-s conditioning pulse (*inset*). Current amplitudes were normalized to the reference peak current elicited from a holding potential of −120 mV. The conditioning and test pulses were separated by a 20 ms hyperpolarization to −120 mV to allow channels to recover from fast inactivation. Smooth curves show χ^2 minimized fits of the data by a Boltzmann function plus a constant term; WT: $V_{1/2} = -64.2 \pm 1.0$ mV, $k = 7.9 \pm 0.5$ mV, $S_0 = 0.16 \pm 0.04$; V445M: $V_{1/2} = -73.6 \pm 1.4$ mV, $k = 6.6 \pm 0.5$ mV, $S_0 = 0.08 \pm 0.01$.

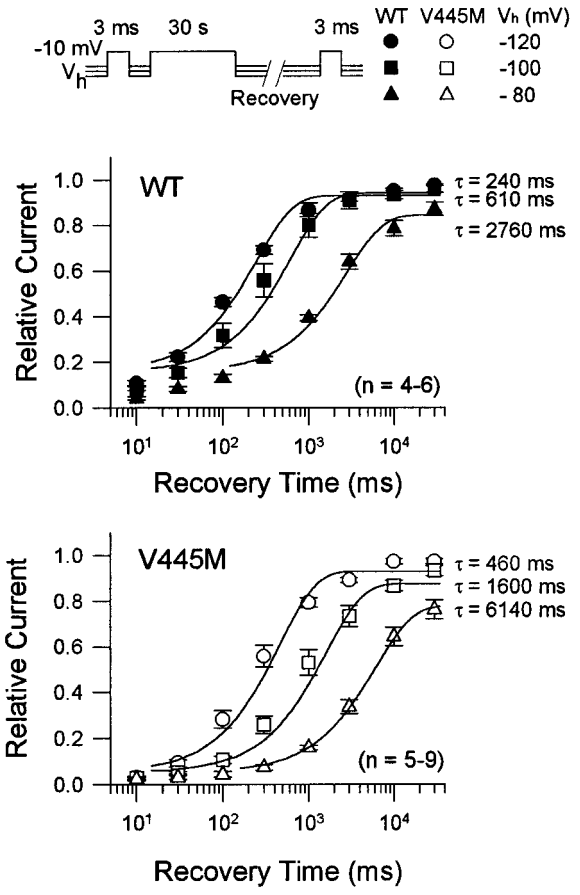

FIGURE 4 Recovery from slow inactivation was slowed for V445M channels. Relative current from WT and V445M channels is plotted as a function of recovery duration on a logarithmic time axis. Inset shows the voltage protocol. Smooth curves are drawn using mean parameter values obtained from χ^2 minimized fits of a single exponential plus a constant (to account for the rapid recovery of channels not slow inactivated) to the data for each cell.

The mean values of the time constant at −120, −100, and −80 mV, obtained from fits to data from 4 to 9 cells, are plotted in Fig. 5 C.

To define further the mechanism by which V445M enhances slow inactivation, we examined the combined kinetic and steady-state behaviors in relation to a two-state model for slow inaction:

$$\text{Not Slow Inactivated} \underset{\beta}{\overset{\alpha}{\rightleftarrows}} \text{Slow Inactivated}$$

The rates of entry (α) and recovery (β) were computed from the relaxation time constant, τ_s, and the fraction of channels not slow inactivated, S_∞, as

$$\alpha = \frac{1}{\tau_s}(1 - S_\infty) \quad \text{and} \quad \beta = S_\infty/\tau_s.$$

The rates are plotted as a function of voltage in Fig. 5 *A*. At potentials negative to −60 mV, the rates vary exponentially with voltage. The major difference between WT and V445M channels is a leftward (negative) shift in the voltage dependence of recovery from inactivation, $\beta(V)$, by about 10 mV. In addition, the entry rate, $\alpha(V)$, is about 1.6-fold faster for V445M. Because a measurable fraction of channels did not become slow inactivated even at depolarized potentials (Fig. 3), both α and β must approach constant nonzero values with increasing membrane voltage. The limiting minimum value of the recovery rate, β_o, is about 0.1 s^{-1} for both WT and V445M channels, as shown directly by the data (squares) at depolarized potentials in Fig. 5 *A*. The corresponding maximal value for $\alpha(V)$ was not evident from the limited voltage range of our rate data ($\leq$ −40 mV). However, the well-defined minimum of the $S_\infty(V)$ data (Fig. 3) and the estimate of the β_o allowed us to compute the maximal entry rate as, $\alpha_o = \beta_o(1 - S_0)/S_0$ which equaled about 0.6 s^{-1} for WT and 1.0 s^{-1} for V445M channels. The curves in Fig. 5 *A* show fits to the rate data by saturating exponential functions of voltage, $\alpha(V) = \alpha_o/[1 + \exp -(V - V_\alpha)/k_\alpha]$ and $\beta(V) = \beta_o[1 + \exp -(V - V_\beta)/k_\beta)]$, with the parameters listed in the legend. The two-state approximation for slow inactivation is supported by the close correspondence between the experimental values of S_∞ and τ_s and the values predicted by the rate relations (lines in Fig. 5 *B* and *C*). We conclude that V445M augments slow inactivation by increasing the entry rate about twofold across all voltages and by shifting the voltage dependence of the recovery rate by −10 mV, which decreases the recovery rate about 2.5-fold at membrane potentials negative to −70 mV.

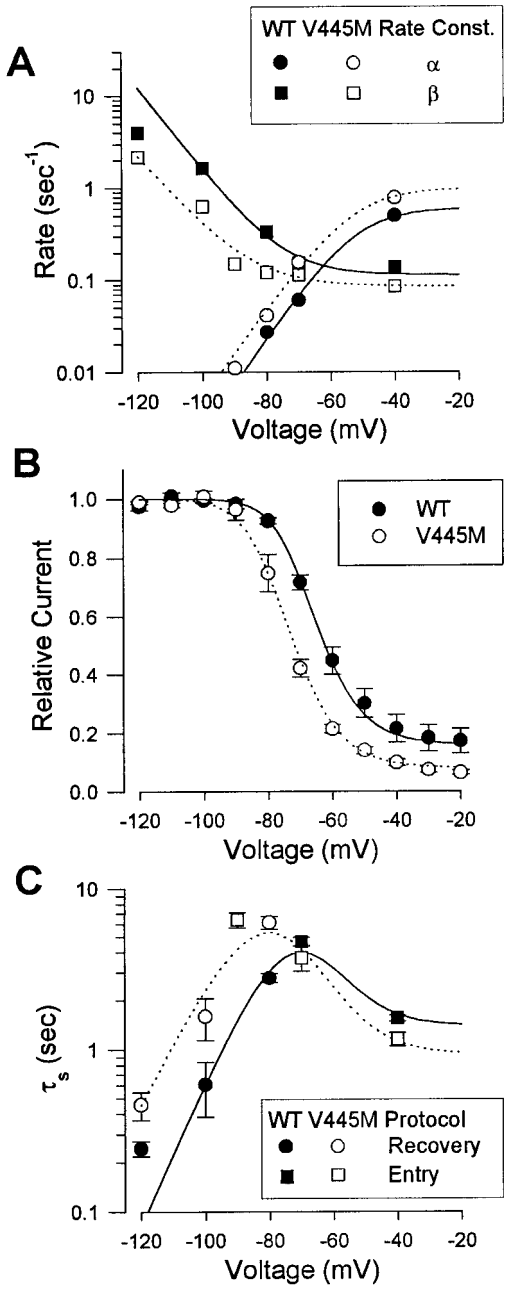

FIGURE 5 The enhanced slow inactivation for V445M was due primarily to a reduced rate of recovery, produced by a left (hyperpolarized) shift in $\beta(V)$. (*A*) The entry (α) and recovery (β) rates were computed from the steady-state, S_∞, and relaxation, τ_s, data as: $\alpha = (1 - S_\infty)/\tau_s$) and $\beta = S_\infty/\tau_s$. The voltage dependencies of the rates were fit to exponential functions that saturated at depolarized potentials: $\alpha(V) = \alpha_o/(1 + e^{-(V-V_\alpha)/k_\alpha})$ and $\beta(V) = \beta_o (1 + e^{-(V-V_\beta)/k_\beta})$. The parameter values were WT: $\alpha_o = 0.60\ s^{-1}$, $V_\alpha = -52.5$ mV, $k_\alpha = 8.6$ mV, $\beta_o = 0.11\ s^{-1}$, $V_\beta = -75.0$ mV, $k_\beta = 9.6$ mV; V445M: $\alpha_o = 0.99\ s^{-1}$, $V_\alpha = -53.3$ mV, $k_\alpha = 9.0$ mV, $\beta_o = 0.086\ s^{-1}$, $V_\beta = -84.9$ mV, $k_\beta = 10.9$ mV. Based on these fits for $\alpha(V)$ and $\beta(V)$, the calculated fraction of channels not slow inactivated ($S_\infty = \beta/(\alpha + \beta)$, lines in *B*) and the calculated time constant ($\tau_s = 1/(\alpha + \beta)$, lines in *C*) are comparable to the data.

Use-dependent inhibition by repetitive pulses

To assess whether the differences in slow inactivation between WT and V445M channels might alter the availability of Na channels in a use-dependent manner, we measured the peaks of Na currents elicited during a train of depolarizations. 20-ms depolarizations to −10 mV were applied at a frequency of 10 Hz from a holding potential of −90 mV. The amplitude of the peak I_{Na} measured during each pulse was normalized by the amplitude of first pulse. The mean of the normalized amplitudes from 8 WT cells and 6 V445M mutants is plotted as a function of the pulse number within a train (Fig. 6). The use-dependent reduction in peak I_{Na} was more pronounced for V445M than WT channels. The augmented use-dependent inhibition for V445M channels is attributable to differences in slow inactivation because recovery from fast inactivation was complete within 80 ms at −90 mV for both WT and mutant V445M channels (data not shown).

DISCUSSION

The gating behavior of heterologously expressed human Na channels was compared for WT and V445M, a missense mutation in the S6 segment of domain I that causes a dominantly inherited from of myotonia. Functional characterization of V445M is of particular interest because none of the other 20 missense mutations in hSkM1 associated with myotonia or periodic paralysis occur in domain I and very few site-directed mutations have been studied in this region. In agreement with a preliminary report by Bennett et al. (1998), we found that the gating of rapid transitions was altered by V445M in a manner that would increase excitability. The persistent Na current was increased, and the

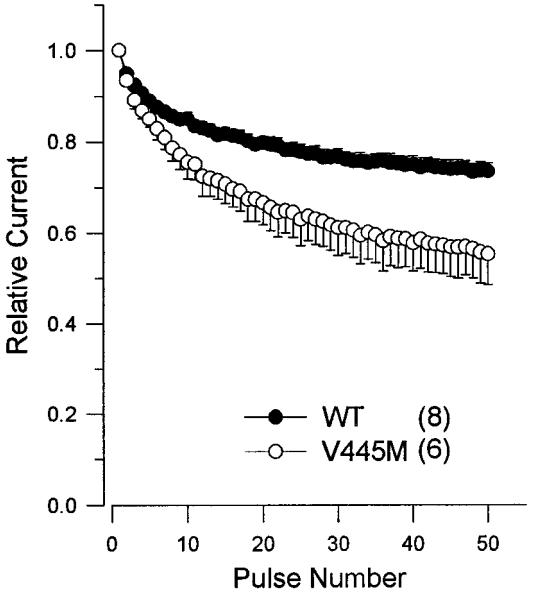

FIGURE 6 Use-dependent reduction of I_{Na} was greater for V445M than WT channels. Sodium currents were elicited by depolarizations to −10 mV from a holding potential of −90 mV. The 20-ms depolarizations were applied at a rate of 10 Hz. The peak current amplitude of each pulse was normalized with respect to the amplitude of the first pulse and plotted against the pulse number.

$G(V)$ curve was left-shifted. The left shift of the $h_\infty(V)$, however, is predicted to reduce the tendency for repetitive myotonic discharges. Like Bennett et al. (1998), we also observed a slowed recovery from inactivation for V445M channels. Our study differs, however, in that we conclude there is no significant difference in recovery from fast inactivation between WT and V445M channels (cf. Fig. 1, 30-ms conditioning pulse). The difference in recovery occurred because slow inactivation was augmented by V445M. At depolarized potentials, slow inactivation was accelerated and was more complete for V445M mutants. Repolarization after prolonged depolarization showed that V445M channels recover about twofold more slowly than WT. The steady-state voltage-dependence of slow inactivation for V445M mutants was more complete and was shifted toward hyperpolarized potentials. In a two-state gating scheme, these changes can be reconciled by a large (10 mV) hyperpolarized shift in the voltage-dependence of the recovery rate and a modest ($\sim$ 1.6-fold) increase in the rate of entry to slow inactivation.

Slow inactivation of the skeletal muscle Na channel has recently been recognized as an important determinant in the propensity for periodic paralysis. Ruff (1994) proposed that a defect of slow inactivation must occur in hSkM1 mutations that cause depolarization-induced periodic paralysis. Otherwise, slow inactivation would shut off the aberrant Na current produced by impaired fast inactivation and the muscle would repolarize. Indeed, slow inactivation is partially disrupted in the two most commonly occurring mutations found in families with HyperPP: T704M (Cummins and Sigworth, 1996; Hayward et al., 1997) and M1592V (Hayward et al., 1997). However, other hSkM1 mutations associated with HyperPP (M1360V) or with PMC in which prolonged episodes of weakness may occur (T1313M, R1448C) have no detectable alteration in slow inactivation (Hayward et al., 1997; Richmond et al., 1997a). Conversely, defects in slow inactivation have never been identified in functional studies of hSkM1 mutants associated with pure myotonia without weakness (Hayward et al., 1997; Richmond et al., 1997b). Based on these results and a model simulation, Hayward et al. (1997) suggested that a defect of slow inactivation increases the likelihood of paralysis but is not a necessary condition. A corollary is that intact slow inactivation might protect against attacks of paralysis. V445M is the only disease-associated mutation of hSkM1 found to enhance slow inactivation. The observation that patients with V445M have painful disabling myotonia, presumably caused by the observed impairment of fast inactivation and left shift of activation (Bennett et al., 1998), but never have attacks of episodic weakness (Rosenfeld et al., 1997) is consistent with our proposed role for slow inactivation. The enhanced slow inactivation of V445M is predicted to reduce the risk of depolarization-induced attacks of weakness, but is still too sluggish to prevent transient runs of repetitive discharges that give rise to myotonic stiffness.

The mechanism by which Na channels slow inactivate and the critical regions of the protein for this process remain unknown. V445M is the second instance of a missense mutation in a Na channel α subunit that enhances slow inactivation. Wang and Wang (1997) reported that slow inactivation is enhanced by a nearby residue in IS6, N434A, in the rat isoform of SkM1 (corresponding to N440 in human SkM1). In contrast, divergent effects on fast gating were observed for mutations in this region. V445M shifted the $G(V)$ relation by -4 mV whereas rN434A caused a $+24$ mV shift, and V445M mildly slowed the rate of fast inactivation (increased the limiting value of τ_h for strong depolarizations) whereas rN434A accelerated fast inactivation nearly twofold. The divergent effects on fast gating processes and the comparable enhancement of slow inactivation implies the cytoplasmic end of IS6 is important for slow inactivation. In addition, the S6 segment is known to contribute to various forms of slow inactivation in other voltage-gated channels. C-type inactivation of *Shaker* K channels is strongly influenced by mutations in S6 (Hoshi et al., 1991; Boland et al., 1994). In Ca channels, variations in inactivation kinetics have been attributed to differences in residues within IS6 or in the flanking extracellular and cytoplasmic regions (Zhang et al., 1994).

An augmentation of slow inactivation has also been observed when fast inactivation is severely disabled, either by internal proteases (Rudy, 1978) or missense mutations within the III-IV loop (Featherstone et al., 1996). The enhanced slow inactivation observed for V445M and rN434A is not likely to be a consequence of altered fast inactivation for several reasons. First, a nearly complete abolition of fast inactivation is required for significant enhancement of slow inactivation. Second, for channels with abolished fast inactivation the augmentation of slow inactivation occurs solely by an increased rate of entry (Rudy, 1978), whereas missense mutations in IS6 dramatically slow the rate of recovery from slow inactivation. Third, the accelerated entry to slow inactivation was several times faster for rN434A than WT channels, after fast inactivation was abolished in both channel types by treatment with chloramine-T. Fourth, we have recently demonstrated that movement of the fast inactivation gate is not tightly coupled to slow inactivation (Vedantham and Cannon, 1998).

Several other regions of the Na channel have been shown to influence slow inactivation. Mutations at the cytoplasmic end of IIS5 (rT698M) or IVS6 (rM1585V) partially disrupt slow inactivation (Cummins and Sigworth, 1996; Hayward et al., 1997). Taken together, the studies on disease-associated missense mutations suggest that a conformational change at the inner vestibule of the pore (cytoplasmic ends of IS6, IIS5, and IVS6) might occur during slow inactivation. On the other hand, slow inactivation is resistant to cytoplasmic application of proteases (Rudy, 1978). Other data have implicated the extracellular face of the channel. Townsend and Horn (1997) demonstrated that slow inactivation of cardiac Na channels is impeded by elevated extracellular levels of alkali metal cations but not by larger

organic cations, suggesting that cation binding near the outer mouth of the pore inhibits closing of the slow inactivation gate. Finally, the voltage-sensing segments are also thought to influence slow inactivation. Slow inactivation appears to be coupled to activation (Ruben et al., 1992), and a mutation in IIS4 of the rat brain IIa channel (L860F) disrupts the slow mode of inactivation in the oocyte expression system (Fleig et al., 1994).

In contrast to fast inactivation, no mutation or physiochemical manipulation has been identified that completely abolishes slow inactivation. This failure may be an ascertainment bias, since fast inactivation is studied more easily and more commonly. A more likely possibility is that slow inactivation does not arise from closure of a single gate or hinged lid. A more global conformational change, involving distant regions of the primary α subunit structure, appears to occur. Whatever the mechanism, our data and that of Wang and Wang (1997) clearly demonstrate that the IS6 region must play a role in slow inactivation.

We thank Al George Jr. for kindly providing the hSKM1 and V445M mammalian expression constructs and Vasanth Vedantham and Jim Morril for comments on the manuscript.

This work was supported by a fellowship from the Klingenstein Foundation (to SCC), the National Institutes of Health (R01-AR42703 to SCC), and the Sumitomo Life Insurance Welfare Services Foundation (to MPT).

REFERENCES

Ackerman, M. J. 1998. The long QT syndrome: ion channel diseases of the heart. *Mayo Clin. Proc.* 73:250–269.

Almers, W., P. R. Stanfield, and W. Stühmer. 1983. Slow changes in currents through sodium channels in frog muscle membrane. *J. Physiol. (Lond.)* 339:253–271.

Bennett, P., D. Wang, P. Ruben, and A. L. George, Jr. 1998. Functional consequences of a D1/S6 sodium channel mutant associated with myotonia. *Biophys. J.* 74:A26.

Boland, L. M., M. E. Jurman, and G. Yellen. 1994. Cysteines in the *Shaker* K^+ channel are not essential for channel activity or zinc modulation. *Biophys. J.* 66:694–699.

Cannon, S. C. 1996. Slow inactivation of sodium channels: more than just a laboratory curiosity. *Biophys. J.* 71:5–7.

Cannon, S. C. 1997. From mutation to myotonia in sodium channel disorders. *Neuromuscul. Disord.* 7:241–249.

Cannon, S. C. 1998. Ion channel defects in the hereditary myotonias and periodic paralyses. *In* Molecular Neurology. J. B. Martin, editor. Scientific American Inc., New York. 257–277.

Cannon, S. C., R. H. Brown, Jr., and D. P. Corey. 1993. Theoretical reconstruction of myotonia and paralysis caused by incomplete inactivation of sodium channels. *Biophys. J.* 65:270–288.

Chandler, W. K., and H. Meves. 1970. Slow changes in membrane permeability and long-lasting action potentials in axons perfused with fluoride solutions. *J. Physiol. (Lond.)* 211:707–728.

Cummins, T. R., and F. J. Sigworth. 1996. Impaired slow inactivation in mutant sodium channels. *Biophys. J.* 71:227–236.

Cummins, T. R., J. Zhou, F. J. Sigworth, C. Ukomadu, M. Stephan, L. J. Ptácek, and W. S. Agnew. 1993. Functional consequences of a Na^+ channel mutation causing hyperkalemic periodic paralysis. *Neuron.* 10: 667–678.

Featherstone, D. E., J. E. Richmond, and P. C. Ruben. 1996. Interaction between fast and slow inactivation in Skm1 sodium channels. *Biophys. J.* 71:3098–3109.

Fleig, A., J. M. Fitch, A. L. Goldin, M. D. Rayner, J. G. Starkus, and P. C. Ruben. 1994. Point mutations in IIS4 alter activation and inactivation of rat brain IIA Na channels in *Xenopus* oocyte macropatches. *Pflügers Arch.* 427:406–413.

George, A. L., Jr., J. Komisarof, R. G. Kallen, and R. L. Barchi. 1992. Primary structure of the adult human skeletal muscle voltage-dependent sodium channel. *Ann. Neurol.* 31:131–137.

Green, D. S., A. L. George, Jr., and S. C. Cannon. 1998. Sodium channel gating defects caused by missence mutations in S6 segments associated with myotonia: S804F and V1293I. *J. Physiol. (Lond.)* 510:685–694.

Hayward, L. J., R. H. Brown, Jr., and S. C. Cannon. 1996. Inactivation defects caused by myotonia-associated mutations in the sodium channel III-IV linker. *J. Gen. Physiol.* 107:559–576.

Hayward, L. J., R. H. Brown, Jr., and S. C. Cannon. 1997. Slow inactivation differs among mutant Na channels associated with myotonia and periodic paralysis. *Biophys. J.* 72:1204–1219.

Hoshi, T., W. N. Zagotta, and R. W. Aldrich. 1991. Two types of inactivation in *Shaker* K^+ channels: Effects of alterations in the carboxy-terminal region. *Neuron.* 7:547–556.

Jurman, M. E., L. M. Boland, Y. Liu, and G. Yellen. 1994. Visual identification of individual transfected cells for electrophysiology using antibody-coated beads. *Biotechniques.* 17:874–881.

McClatchey, A. I., S. C. Cannon, S. A. Slaugenhaupt, and J. F. Gusella. 1993. The cloning and expression of a sodium channel β_1-subunit cDNA from human brain. *Hum. Mol. Genet.* 2:745–749.

Mitrovic, N., A. L. George, Jr., H. Lerche, S. Wagner, C. Fahlke, and F. Lehmann-Horn. 1995. Different effects on gating of three myotonia-causing mutations in the inactivation gate of the human muscle sodium channel. *J. Physiol. (Lond.)* 487:107–114.

Plassart-Schiess, E., L. Lhuillier, A. L. George, Jr., B. Fontaine, and N. Tabti. 1998. Functional expression of the Ile693Thr Na^+ channel mutation associated with paramyotonia congenita in a human cell line. *J. Physiol. (Lond.)* 507:721–727.

Richmond, J. E., D. E. Featherstone, and P. C. Ruben. 1997a. Human Na^+ channel fast and slow inactivation in paramyotonia congenita mutants expressed in *Xenopus laevis* oocytes. *J. Physiol. (Lond.)* 499:589–600.

Richmond, J. E., D. VanDeCarr, D. E. Featherstone, A. L. George, Jr., and P. C. Ruben. 1997b. Defective fast inactivation recovery and deactivation account for sodium channel myotonia in I1160V mutant. *Biophys. J.* 73:1896–1903.

Rosenfeld, J., K. Sloan-Brown, and A. L. George, Jr. 1997. A novel muscle sodium channel mutation causes painful congenital myotonia. *Ann. Neurol.* 42:811–814.

Ruben, P. C., J. G. Starkus, and M. D. Rayner. 1992. Steady-state availability of sodium channels. Interactions between activation and slow inactivation. *Biophys. J.* 61:941–955.

Rudy, B. 1978. Slow Inactivation of the sodium conductance in squid giant axons: pronase resistance. *J. Physiol. (Lond.)* 283:1–21.

Ruff, R. L. 1994. Slow Na^+ channel inactivation must be disrupted to evoke prolonged depolarization-induced paralysis. *Biophys. J.* 66: 542–545.

Ruff, R. L., L. Simoncini, and W. Stühmer. 1988. Slow sodium channel inactivation in mammalian muscle: a possible role in regulating excitability. *Muscle Nerve.* 11:502–510.

Townsend, C., and R. Horn. 1997. Effect of alkali metal cations on slow inactivation of cardiac Na^+ channels. *J. Gen. Physiol.* 110:23–33.

Vedantham, V., and S. C. Cannon. 1998. Slow inactivation does not affect movement of the fast inactivation gate in voltage-gated Na^+ channels. *J. Gen. Physiol.* 111:83–93.

Wang, S.-Y., and G. K. Wang. 1997. A mutation in segment I-S6 alters slow inactivation of sodium channels. *Biophys. J.* 72:1633–1640.

Zhang, J. F., P. T. Ellinor, R. W. Aldrich, and R. W. Tsien. 1994. Molecular determinants of voltage-dependent inactivation in calcium channels. *Nature.* 372:97–100.